Selective enrichment of phosphorylated peptides by monolithic polymers surface imprinted with bis-imidazolium moieties by UV-initiated cryopolymerization

Liu, Mingquan; Torsetnes, Silje Bøen; Wierzbicka, Celina; Jensen, Ole Nørregaard; Sellergren, Börje; Irgum, Knut

Published in:
Analytical Chemistry

DOI:
10.1021/acs.analchem.9b02211

Publication date:
2019

Document version:
Accepted manuscript

Citation for pulished version (APA):
Liu, M., Torsetnes, S. B., Wierzbicka, C., Jensen, O. N., Sellergren, B., & Irgum, K. (2019). Selective enrichment of phosphorylated peptides by monolithic polymers surface imprinted with bis-imidazolium moieties by UV-initiated cryopolymerization. *Analytical Chemistry*, *91*(15), 10188-10196. https://doi.org/10.1021/acs.analchem.9b02211

Article

Selective Enrichment of Phosphorylated Peptides by Monolithic Polymers Surface Imprinted with *bis*-Imidazolium Moieties by UV-initiated Cryopolymerization

Mingquan Liu, Silje Bøen Torsetnes, Celina Katarzyna Wierzbicka, Ole Nørregaard Jensen, Börje Sellergren, and Knut Irgum

Anal. Chem., **Just Accepted Manuscript** • DOI: 10.1021/acs.analchem.9b02211 • Publication Date (Web): 24 Jun 2019

analytical chemistry

Article

Cite This: *Anal. Chem.* 2019, 91, ####-####

pubs.acs.org/ac

Selective Enrichment of Phosphorylated Peptides by Monolithic Polymers Surface Imprinted with *bis*-Imidazolium Moieties by UV-initiated Cryopolymerization

Mingquan Liu[a], Silje Bøen Torsetnes[b¶], Celina Wierzbicka[c], Ole Nørregaard Jensen[b], Börje Sellergren[c], Knut Irgum[a]*

a) Umeå University, Department of Chemistry, S-901 87 Umeå, Sweden.
b) University of Southern Denmark, Department of Biochemistry & Molecular Biology and VILLUM Center for Bioanalytical Sciences, Campusvej 55, DK-5230 Odense M, Denmark.
c) Malmö University, Department of Biomedical Sciences, Faculty of Health and Society, S-205 06 Malmö, Sweden.

Supporting Information

ABSTRACT: Reversible protein phosphorylation on serine, threonine, and tyrosine residues is essential for fast, specific, and accurate signal transduction in cells. Up to now, the identification and quantification of phosphorylated amino acids, peptides and proteins continue to be one of the significant challenges in contemporary bioanalytical research. In this paper, a series of surface grafted monoliths in the capillary format targeting phosphorylated serine have been prepared by first synthesizing a monolithic core substrate material based on trimethylolpropane trimethacrylate, onto which a thin surface-imprinted layer was established by oriented photografting of a variety of *mono*- and *bis*-imidazolium host monomers at sub-zero temperature, using six different continuous or pulsed UV light sources. The imprinted monolith capillaries were evaluated in a capillary liquid chromatographic system connected to a mass spectrometer in order to test the specific retention of phosphorylated peptides. Site-specific recognition selectivity and specificity for phosphorylated serine was demonstrated when separating amino acids and peptides, proving that the optimized materials could be used as novel trapping media in affinity-based phosphoproteomic analysis.

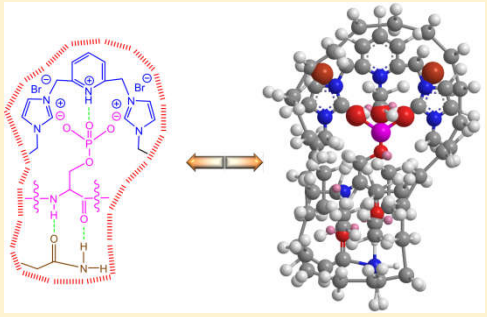

The ability of living cells to rapidly change their gene expression pattern in response to stimuli usually involves modulation of the activity of pre-existing transcription factors. The abundant and intriguing reversible protein phosphorylation and dephosphorylation on serine, threonine, and tyrosine (S/T/Y) has been identified as a major regulatory post-translational modification (PTM) in both prokaryotic and eukaryotic cells, of profound importance to transcription factor activity regulation.[1,2] Defects or mutations in the deregulation of phosphorylation have been implicated as a major cause of a variety of diseases, including diabetes, neurodegeneration, and cancer.[3-5] Given the vital role of phosphorylation in the overall cell regulation, the systematic characterization of the phosphoproteome, including determination of the specific site(s) of phosphorylation within the protein of interest, are therefore crucial to develop a more complete understanding of the protein modifications role in the early stages and progression of disease, and to explore novel precautionary and therapeutic strategies for the corresponding disease treatment.[6] Roughly 30 % of all proteins in mammalian organisms are phosphorylated and serine residues account for approximately 90 % of the total cellular phosphorylation, while threonine and tyrosine residues are estimated at about 10 and 0.1 %, respectively.[7] In this context, a comprehensive mapping of the phosphoproteome targeting phosphoserine is therefore significant in order to understand cellular processes, as well as disease mechanism and therapy.

A variety of strategies have been established assisted by mass spectrometry (MS) for separation and analysis of phosphopeptides, including co-precipitation,[8] chemical derivatization,[9] ion exchange chromatography,[10] inorganic salt affinity chromatography,[11] metal oxide affinity chromatography (MOAC),[12] immobilized metal affinity chromatography (IMAC),[13] and immunoaffinity.[14] This steadily growing array of phospho-selective enrichment techniques implies that current methods are still far from perfect. Chemoaffinity protocols, although widely used in phosphoproteomics, lack site selectivity for phosphorylation at serine (**pS**), threonine (**pT**), or tyrosine (**pY**)[15,16] and exhibit a sequence bias in favor of peptides rich in negatively charged aspartic and glutamic acids. Furthermore, these methods generally require sample amounts in the milligram range and complex protein digesting steps.[17,18] An alternative is immuno-based approaches, which are commonly utilized for fractionation at the protein or peptide level. Antibodies with high affinity for **pY** peptides have been developed, but these are costly and fragile, and show an undesirable cross-selectivity. Meanwhile, antibody-based enrichment and isolation of **pT** and even the abundant **pS**-containing peptides has not yet been routinely possible due to the lower immunogenicity of the **pT** and **pS** side chains.[19,20]

Molecular imprinting is a polymerization scheme used to produce biomimetic "synthetic antibody" receptors. The resulting molecularly imprinted polymers (MIPs) are capable of tailored specific molecular recognition and binding of target molecules with affinities and specificities similar to natural enzymes and antibodies,[21,22] providing robust and cost-efficient alternatives to biologically derived receptors and antibodies.[23,24] MIPs are generally synthesized by co-polymerizing functional and cross-linking monomers in the presence of a molecular template carrying an epitope against which selectivity is sought. Subsequent removal of the template leaves the polymer

network with binding sites complementary in shape, size, and functional group orientation which are able to rebind the template molecule with affinity and selectivity comparable to those of biological receptors.[25-28] "Synthetic antibodies" specifically targeting **pS**-containing amino acids or phosphopeptides could therefore become an important addition to the proteomics tool chest.[29]

Monolithic materials with micrometer scale through-pores and nanometer scale mesopores are important materials in separation science, also as molecular imprinting substrates.[30, 31] We reported, *e.g.*, recently on mesoporous MIP monoliths with selectivity against phosphopeptides formed by step-growth polymerization of melamine-formaldehyde.[32] A drawback of this formation of molecularly imprinted monolith surfaces by direct polymerization in the presence of a MIP template, is that the porogen composition have to be optimized for each MIP template to arrive at similar porous properties. A more versatile tactic is therefore a two-step approach, based on polymerizing a suitable monolithic substrate with well-defined porous properties and anchoring groups on its pore surfaces, followed by grafting of a MIP layer by aid of these groups. Provided the graft-imprinted surface layer is kept sufficiently thin, its influence on the column permeability will be minute. Thin grafting layers also prevent deep template embedment, which leads to poor analyte recognition and large diffusion barriers in bulk polymerized MIPs.[33-35] The monolithic route devised here is fast and convenient compared to the time-consuming and complicated crushing, sieving, and packing procedures needed with bulk polymerized MIPs. As part of our continued efforts to develop monolithic plastic antibodies in the capillary format with extended solvent compatibility for phosphoproteomics, we here present a series of surface imprinted materials with site-specific **pS** recognition capabilities prepared by oriented UV-initiated cryopolymerization. The versatility of the prepared monolithic columns is demonstrated by selective extraction of **pS**-containing analytes from samples of varying complexity.

MATERIALS AND METHODS

Reagents and Materials. The monomers 2-propenamide (acrylamide; AAm), 2,2-bis(prop-2-enoyloxymethyl)butyl prop-2-enoate (trimethylolpropane trimethacrylate; TRIM), [2-(hydroxymethyl)-3-prop-2-enoyloxy-2(prop-2-enoyloxymethyl)propyl] prop-2-enoate (pentaerythritol triacrylate; PETA) were purchased from Sigma-Aldrich (Steinheim, Germany), as were the tetrabutylammonium hydroxide (TBAOH; 1 M in methanol), the deuterated acetonitrile-d_3 (CD_3CN, >99.8 atom % D), and the α-casein (bovine). The 2,2,4-trimethylpentane (isooctane) and dry toluene were from Fischer (Zürich, Switzerland), and the acetone and 4-(2-hydroxyethyl)-1-piperazineethanesulfonic acid (HEPES) were from VWR (Radnor, PA, USA). The 2-methoxy-2-phenylacetophenone (benzoin methyl ether; BME), 2,2-diphenyl-1-picrylhydrazyl (DPPH), 3-[(methacryloyl)oxypropyl]trimethoxysilane (γ-MAPS), and 2,2'-azobis[2-methyl- propanenitrile (2,2'-azobisisobutyronitrile; AIBN) were purchased from Fluka (Buchs, Switzerland). Acetonitrile (ACN) and dry methanol (MeOH) were from J. T. Baker (Phillipsburg, NJ, USA) and trifluoroacetic acid (TFA) was from Merck (Darmstadt, Germany). The human Angiotensin II octapeptides DRVYIHPF and DRVSIHPF were from Fluka (Buchs, Switzerland) and their phosphorylated modifications DRV**pY**IHPF and DRV**pS**IHPF were custom synthesized by LifeTein LLC (Hillsborough, NJ, USA). The Fmoc [Fmoc = (9-fluorenylmethyl) carbamate] modified amino acids Fmoc-Y-OH and Fmoc-S-OH, and their phosphorylated counterparts Fmoc-**pY**-OH and Fmoc-**pS**-OH were purchased from Bachem GmbH (Bubendorf, Switzerland).

The template *N*-(9-fluorenylmethyloxycarbonyl)-*O*-phosphonoserine ethyl ester (Fmoc-**pS**-OEt) was synthesized as in our recent reports.[32, 35] All chemicals were used as received, unless otherwise noted. The water used was prepared by Milli-Q equipment from Merck Millipore (Bedford, MA, USA) and had a resistivity of > 18 MΩ·cm^{-1}. The cationic imidazolium (IMI) functional monomers in Figure 1 were synthesized according to published procedures.[35-37]

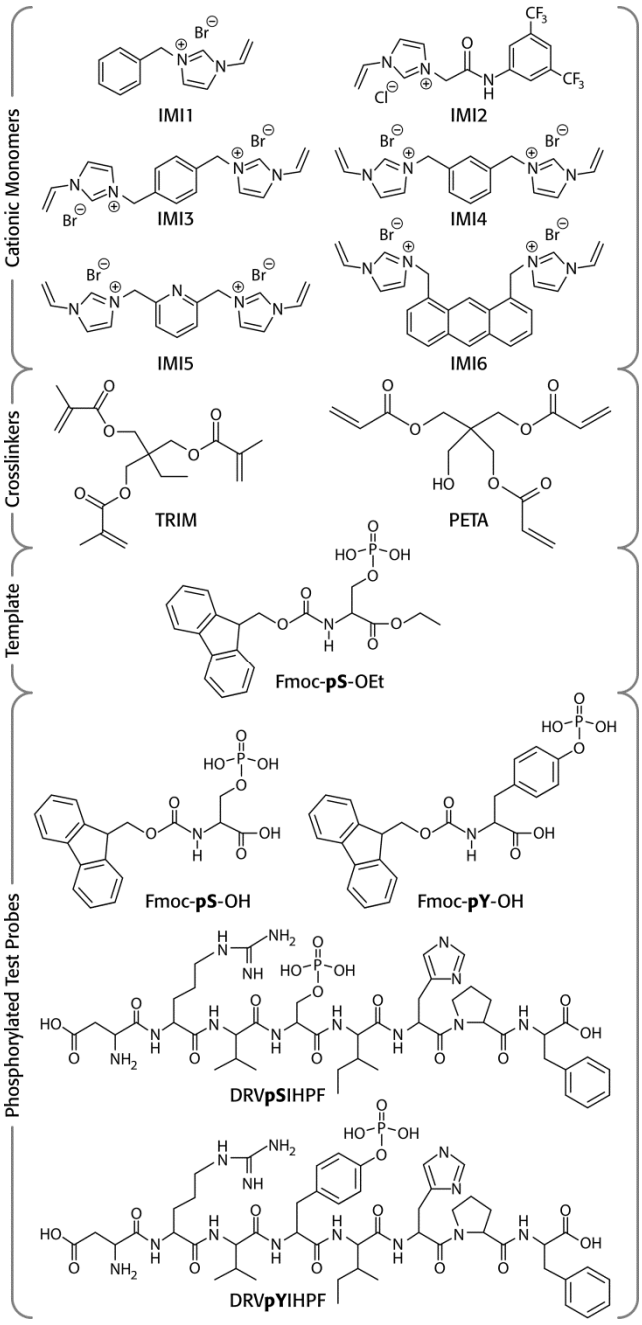

Figure 1. Chemical structures of the cationic monomers IMI1–IMI6, the crosslinkers TRIM and PETA, the phosphorylated Fmoc-**pS**-OEt target used to prepare surface imprinted monoliths selective towards phosphoserine, and the phosphorylated variants of the utilized test probes, Fmoc-**pS**-OH, Fmoc-**pY**-OH, and the octapeptides DRV**pS**IHPF and DRV**pY**IHPF. Their corresponding non-phosphorylated test probes Fmoc-S-OH, Fmoc-Y-OH, DRVSIHPF and DRVYIHPF only lack the phosphate groups on serine or tyrosine, and are therefore not drawn.

Preparation of Core TRIM Monoliths. The monolithic capillary columns were prepared in fused silica capillaries (250 μm i.d. × 360 μm o.d.) with UV transparent fluoropolymer coating, from Polymicro Technology (Phoenix, AZ, USA). In order to covalently anchor the polymeric monoliths to the inner wall, the capillaries were pretreated to introduce methacrylic anchoring groups.[34] Briefly, the capillaries

were washed with acetone and deionized water, then a 1 M NaOH aqueous solution was flushed through the capillary for approximately 5 min, where after the capillary was sealed in the filled state with rubber at both ends. The capillaries were etched by heating in a circulating air oven at 100 °C for 2 h, and cooled to room temperature. A washing procedure with deionized water followed by acetone (15 min each) was employed and the final drying took place by a flow of dry nitrogen for at least 1 h. Methacrylic anchoring groups were introduced onto the capillary inner wall by filling the capillary with a mixture of γ-MAPS in DMF (1:1, v/v) containing 0.05 % DPPH as polymerization inhibitor. The capillaries were sealed as above and heated at 100 °C for 6 h. The capillaries were thereafter washed with acetone and dried in a vacuum oven at 60 °C for at least 3 h. Finally, the vinylized capillaries were cooled to room temperature and purged with a flow of dry nitrogen for at least 1 h. Most capillaries were used directly after pretreatment; otherwise, they were stored in a desiccator for further use.

A small library of core TRIM capillary monoliths (Table S-1) was prepared using homogenous degassed precursor solutions containing 40 % (w/w) TRIM with isooctane/toluene mixtures at six different weight ratios as diluent and porogen. AIBN (1 % with respect to the weight of the TRIM) served as initiator for the photo-polymerization. The aforementioned γ-MAPS activated capillary was cut into 90 mm long pieces that were filled by inserting one of its ends through a pre-pierced PTFE-lined septum of glass vial containing the corresponding monomer/porogen cocktail and the other end inserted into an empty septum-capped vial. Capillary force and a slight overpressure of N_2 (g) applied to the vial containing the monomer cocktail caused a slow flow, while care was taken to maintain the capillary end submerged so that no gas bubbles were trapped in the capillary. After several drops of monomer cocktail had been transferred to the empty vial, the N_2 pressure was released from the vial containing the monomer cocktail and both vials were taken to atmospheric pressure by momentarily piercing their septa by hypodermic needles. The filled capillary/vial assemblies were thereafter immediately mounted on a model KP282 cold plate from Fryka Kältetechnik (Esslingen, Germany) for temperature control and subjected to photoinitiated cryopolymerization at –10 °C using one of the six different UV radiation sources (see below). The radiation intensity in the photo-polymerization zone was determined by an International Light Model IL1400 radiometer (Newburyport, MA, USA) equipped with a model XRL140B probe and the polymerization times were adjusted so that all polymerizations were carried out with a radiation dose of 10 ± 1 J/cm^2.

The UV radiation sources used in the photo-cryopolymerization were either continuous and pulsed; the four continuous light polymerization units were: A) A CureZone (UV Process Supply, Chicago, IL, USA) UV irradiation chamber equipped with a 400 W quartz-lined mercury lamp, with a 4 mm thick float glass sheet positioned between the lamp and the capillary/vial assemblies to remove radiation below ≈ 320 nm; B) A 15 W BLB lamp (Sankyo Denki Co., Ltd., Tokyo, Japan), placed at 50 mm distance from, and aligned with, the capillary/vial assemblies; C) A UV Spectrolinker XL-1500 (Spectronics Corporation, Westbury, NY, USA) fitted with six 15 W BLB blacklight tubes; D) A JD-230 Gel Curing UV Lamp (Yayuo Jiadi Electrical Factory, Zhejiang, China) with four 9 W fluorescent tubes having emission maximum around 370 nm. The two pulsed light units were: E) A CoolCure XL 4.2 high intensity pulsed xenon lamp with an RC-742 power unit (XENON Corporation, Wilmington, MA, USA), controlled by a custom-made Raspberry Pi console unit; and F) A Philips XOP 15 O/F 1500 W linear low pressure non-ozone-producing xenon discharge lamp (D.T.S., Misano Adriatico, Italy). In this lamp, the 240 V/50 Hz mains is connected directly to the main electrodes of the discharge tube, which is ignited through a trigger transformer using a 5 μF capacitor charged to 320 V. The intensity and duration of the pulse is varied by the trigger delay; the earlier in the 10 mS half pulse of the 50 Hz supply, the longer and more intense the pulse. Polymerization was done at maximum trigger rate and intensity, yielding pulses of ≈ 3 ms duration at 12.5 Hz repetition rate. Prior to use, each UV lamp had been warmed up around 3 h to ascertain constant temperature and intensity during the course of the photo-cryopolymerization period.

After the polymerization was completed, the capillaries were detached from the vials, which were disintegrated with minimal force to render the bulk monolithic materials formed there as intact as possible. The bulk monolithic materials thus recovered were cut into roughly cubiform pieces with approximately 2-3 mm sides and transferred to cellulose extraction thimbles, which were Soxhlet extracted in tetrahydrofuran for 72 h to remove the porogens, oligomeric material, and unpolymerized monomers. The Soxhlet-extracted bulk TRIM monolithic materials were finally dried under reduced pressure (≈ 100 Pa) in a Gallenkamp (Loughborough, UK) vacuum oven at 110 °C for at least 6 h prior to further characterization. The TRIM monolithic capillaries, with 1 mm pieces trimmed from each end to remove eventual blockages or voids, were cleaned by pumping with methanol for at least 2 h at 20 μL/min.

Establishment of Molecularly Imprinted pS Sites by Surface Grafting. The mixtures used in the photograft imprinting were prepared as optimized in our previous work.[35, 38] Specifically, the template Fmoc-**pS**-OEt (7.8 μmol), chosen to produce **pS** site-specific recognition specificity, was mixed with two equivalents of the strong base TBAOH to form the corresponding *bis*-TBA phosphate salt *in situ*. This anionic **pS** template was then mixed with a series of cationic *mono*- and *bis*-imidazolium functional host monomers (15.6 μmol of *mono*-imidazolium or 7.8 μmol of *bis*-imidazolium monomers), with acrylamide (6.5 μmol) as co-monomer and PETA (98.9 μmol) as crosslinker, in 956 μL of a 1:1 (v/v) mixture of dry toluene and dry methanol. After adding BME (1 % w/w with respect to the combined monomer weight) as photoinitiator, the grafting solutions were finally given a brief purge with nitrogen to remove dissolved oxygen. The corresponding non-imprinted reference polymers (NIPs) were prepared as described above, but with the Fmoc-**pS**-OEt *bis*-TBA template omitted from the grafting mixtures. At least twenty column volumes of these grafting solutions were thereafter introduced into the TRIM24 core monolith capillary substrates using a syringe pump. The filled capillaries were then sealed with GC rubber septa and frozen at –70 °C by clamping between two blocks of solid carbon dioxide for 1 h. From there the capillaries were rapidly transferred onto the cooling plate and photo-grafted at –10 °C by one of the six UV radiation sources to establish a thin imprinted grafting layer. The integrated UV radiation was set to 11 ± 1 J/cm^2 by varying the reaction time, as explained above. After the photografting was completed, the resultant NIP and MIP capillaries were individually flushed by methanol containing 0.1 % HBr or HCl aqueous solution at 20 μL/min for at least 6 h before further evaluation. The back pressures of each monolith were recorded before grafting and during the washing steps, and capillary monoliths which did not show an increase in back pressure of 400 ± 100 kPa compared to that measured prior to grafting were discarded.

Characterization and Evaluation. Experimental procedures and results from the characterization and evaluation of the monolith MIP and NIP capillaries, consisting of porosity assessment by nitrogen cryosorption and mercury intrusion, field emission scanning electron microscopy (FE-SEM), Fourier-transform infrared (FT-IR) spectroscopy, X-ray photoelectron spectroscopy (XPS), suspended-state and saturation transfer difference high-resolution magic-angle-

spinning nuclear magnetic resonance (STD HR/MAS NMR), capillary liquid chromatography, and thermogravimetric analysis (TGA) can be found in the Supporting Information.

RESULTS AND DISCUSSION

Materials Characterization. The TRIM substrate, and the non-imprinted (NIPs) and imprinted (MIPs) based on this monolith recipe were characterized by N_2 cryosorption and Hg intrusion to chart their porosity. The chosen TRIM24 monolith and the MIPs and NIPs based thereon were in addition subjected to FE-SEM to visualize their morphologies, FT-IR and XPS for determining their chemical composition, STD-NMR to probe interaction patterns, TGA to explore and compare the thermal stability, and their flow-dependent back pressure in three different solvents. For space reason, the results from these characterizations are shown Figures S-1 to S-8 and Tables S-1 to S-3 in the Supporting Information, along with the accompanying experimental descriptions. References to Figures and Tables numerated by an initial S in the following text refer to the data located there.

Optimization of the TRIM Monolithic Substrate Synthesis. The porous structure is a central optimization criterion for monolithic capillary support substrates to be used in affinity chromatography. Desirable properties are a surface area sufficiently large to provide the required sample capacity, and a high permeability which will allow operation at reasonably low pressure. In the current study, we chose TRIM as monomer for the monolithic substrate, since it produces a strong crosslinked network with residual polymerizable methacrylic groups on the pore surfaces. The key variables were the monomer amount together with the composition of inert porogenic solvents in the polymerization mixture, which allowed a tuning of the pore size over at least two orders of magnitude from tens to thousands of nanometers, producing porous structures with specific surface area and macropores sufficiently large to create the required capacity and allow operation at a reasonably low pressure. In scouting experiments, we found that fixing the TRIM concentration at 40 % (w/w) allowed us to adjust the specific surface area and pore size distribution by varying the ratio of the toluene porogen and the isooctane diluent. Furthermore, the bulk polymers recovered from the vials appeared in most cases to be white and rigid monoliths in the dry state (Table S-1), which was expected since 40 % (w/w) of the hexafunctional TRIM monomer should produce monolithic materials with the rigidity and mechanical stability necessary for flow applications with polymerizable groups abundant on the surfaces.

A variety of solvents were considered as porogens in the monolith synthesis. After taking into account the boiling points, monomer solubility, and lack of reactivity with monomer, we ended up with the "standard" combination of toluene and isooctane. This choice was also based on an ability to tune the porous properties over a wide range, discovered in initial experiments (data not shown). Among these porogens, isooctane acts as thermodynamically poor solvent for the growing polymer chains, while toluene is a good (or at least better) solvent with respect to the polymer. The thermodynamic quality of the porogen mixture can therefore be tuned by varying their ratio, which was done at six different levels spanning from zero to 100 % volume percent of in steps of 20 %.

The photopolymerization utilized throughout this study has several advantages over the more conventional thermal initiation processes. It significantly reduces the polymerization time from hours to minutes and allows the use of more volatile porogenic solvents since photopolymerizations are typically carried out at lower temperature. A variety of light sources can be used for photopolymerization. In an attempt to further tune the porous structure and improve the structural homogeneity of the TRIM monoliths, we therefore evaluated six different UV light sources producing either pulsed or continuous light, resulting in a library of in total thirty-six TRIM monoliths covering a wide range of meso- and macroporous properties. Special care was taken to ascertain identical temperatures and radiation doses in the syntheses. A polymerization temperature of –10 °C was chosen to strengthen temperature-sensitive intermolecular interactions, by thermostatting the capillaries on a cold stage to minimize heating from the UV source and the exothermic polymerization reaction. Applying the same integrated UV radiation regardless of source was chosen instead of running the polymerizations for equal duration since the extent of the UV-initiated polymerization is controlled by dose-dependent photolytic initiator cleavage.

Qualitative morphology assessments of the bulk phase monolithic materials synthesized alongside the capillary monoliths are shown in Table S-1, with the specific surface areas, total pore volumes, and average mesopore sizes determined by multipoint nitrogen cryosorption, and the median macropore sizes corresponding to the most prominent peak in differential mercury intrusion porosimetry measurements. The main finding is that the specific surface area of the obtained materials increased gradually with the toluene content in the mixed porogen and started to level off when the toluene:isooctane ratio was 60/40. This was accompanied by the expected decrease in both meso- and macropore size. At 80/20 and beyond, the materials were no longer recovered as robust white solids, but instead appeared as opaque and glass-like, fluffy, or granulous solids. A somewhat surprising observation is the tight correlation (Pearson $r^2 = 0.9967$) seen between the average mesopore size measured by nitrogen cryosorption and the median macropore size measured by mercury intrusion porosimetry (Figure S-2), in spite of a difference in size between these pore families of nearly a hundred times. Meso- and macropores should be formed by different processes, and the measurements of meso- and macropores are based on radically different principles.[39] The tight correlation might be related to the photopolymerization procedure, but we report this merely as an incidential observation and will refrain from discussing this further here.

Based on the macroporosity, the mesopore size distribution (*cf.* isotherms in Figure S-1), specific surface area, and the linear and hysteresis-free back-pressure *vs.* flow rate plots (Figure S-4), we chose as grafting substrate for the molecular imprinting of phosphopeptides the TRIM24 monolith recipe, which was polymerized for 20 min with the Philips XOP 15 O/F 1500 W xenon discharge lamp using a toluene:isooctane ratio of 60:40. Repeatable and stable meso- and macroporosities, specific surface areas, and back-pressure measurements (data not shown) warrant that the TRIM24 substrate could be prepared with repeatable macroporosity, and the back-pressure measurements (Figure S-4) showed no swelling tendency in the tested solvents.

Optimization of the Molecular Imprinting Process. A drawback of monolithic MIP preparation by direct polymerization in the presence of template, is an inferior template recognition performance owing to buried recognition sites,[35] but also the tedious optimizations required to find the desired meso- and macroporosity combination for each new set of monomers. A way to address both these shortcomings is to employ a two-step scheme, where a monolithic substrate with optimized porous properties is subjected to molecular imprinting by surface photografting. Specifically, we evaluated six different custom synthesized cationic imidazolium-based functional monomers for the imprinting of *N*-Fmoc *O*-ethyl protected phosphoserine targeting the **pS** epitope onto TRIM substrates by means of photoinitiated cryografting.[35] Acrylamide was used as neutral co-monomer to enhance the hydrogen bonding potential of the imprinted cavities and

trivinylic PETA was chosen as crosslinker to produce a rigid surface imprinted layer, in order to prevent collapse of the mesopore space.

Table 1. Retention and imprinting parameters of MIP monoliths.

MIP	Monomer	UV Source	k'	IF [a)]	SF [b)]	I [c)]
MIP 01	IMI1	A	2.1	1.28	0.66	0.55
MIP 02	IMI1	B	2.3	1.45	0.64	0.51
MIP 03	IMI1	C	2.4	1.40	0.74	0.63
MIP 04	IMI1	D	2.5	1.34	0.63	0.59
MIP 05	IMI1	E	2.7	1.36	0.59	0.57
MIP 06	IMI1	F	2.4	1.31	0.67	0.64
MIP 07	IMI2	A	5.0	1.63	0.66	0.57
MIP 08	IMI2	B	5.0	1.62	0.72	0.61
MIP 09	IMI2	C	5.0	1.58	0.77	0.69
MIP 10	IMI2	D	5.4	1.69	0.73	0.64
MIP 11	IMI2	E	6.3	1.99	0.62	0.53
MIP 12	IMI2	F	5.2	1.65	0.69	0.68
MIP 13	IMI3	A	10.4	2.11	0.85	0.82
MIP 14	IMI3	B	11.0	2.29	081	0.79
MIP 15	IMI3	C	11.5	2.23	088	0.88
MIP 16	IMI3	D	11.5	2.32	0.89	0.91
MIP 17	IMI3	E	10.9	2.16	0.84	0.86
MIP 18	IMI3	F	11.0	2.31	0.82	0.83
MIP 19	IMI4	A	20.5	2.85	0.86	0.83
MIP 20	IMI4	B	18.3	2.66	0.85	0.85
MIP 21	IMI4	C	20.3	2.35	0.90	0.90
MIP 22	IMI4	D	22.4	2.91	0.92	0.93
MIP 23	IMI4	E	18.5	2.88	0.88	0.89
MIP 24	IMI4	F	20.4	2.39	0.84	0.84
MIP 25	IMI5	A	26.3	3.05	0.91	0.89
MIP 26	IMI5	B	29.5	3.03	0.89	0.87
MIP 27	IMI5	C	31.3	3.02	0.92	0.93
MIP 28	IMI5	D	31.7	3.71	0.93	0.96
MIP 29	IMI5	E	29.1	2.96	0.90	0.90
MIP 30	IMI5	F	32.9	3.11	0.87	0.87
MIP 31	IMI6	A	19.2	2.97	0.85	0.87
MIP 32	IMI6	B	18.1	2.89	0.79	0.81
MIP 33	IMI6	C	28.2	3.08	0.87	0.89
MIP 34	IMI6	D	27.0	3.26	0.91	0.92
MIP 35	IMI6	E	18.4	2.71	0.82	0.83
MIP 36	IMI6	F	25.3	2.86	0.86	0.82

a) Imprinting factor IF = k'_{MIP}/k'_{NIP}; b) Selectivity factor SF = $k_{Analogue}/k_{Template}$; c) Relative imprinting factor I = $IF_{Analogue}/IF_{Template}$.

By varying the ratio of the toluene and methanol used as binary grafting porogen, we were able to synthesize materials with thin grafting layers that largely preserved the mesoporous properties of the TRIM substrate monolith while maximizing the amount of accessible surface-imprinted sites. The MIP precursor mixture composition and the photografting procedure were optimized based on extensive scouting experiments. The grafting step temperature was varied between –20 to 20 °C and the results indicated that –10 °C led to well-behaved imprinted layers in a reasonable radiation time. The imprinting cocktail composition (the ratios of template to imidazolium monomer, ancillary monomer to crosslinker, total monomers to porogens, and the amount of initiator) was based on experience from our previous work with imidazolium monomers in phosphopeptide imprinting.[35] With these ratios fixed, the porogen ratio and the UV sources were left as variables, yielding again a library of thirty-six monoliths imprinted on the TRIM24 substrate covering a full range of MIPs with phosphorylated serine recognition properties as listed in Table 1. From the retention and imprinting parameter results presented there, it can be observed that the both the type of imidazolium host functional monomer and the UV radiation source have noticeable influence on the selectivity of the surface imprinted capillary monolithic columns. This is in agreement with our previous reports on imidazolium based receptors for phosphotyrosine[35] and phospholipids[36]. Hence, monocationic host monomers interact more weakly than *bis*-cationic hosts accounting for the weaker retention and lower IF for IMI1-IMI2 *versus* IMI3-5. Comparing *bis*-imidazolium receptors made of IMI3 and IMI4 featuring the imidazolium groups bridged by meta- or para-substituted xylyl groups the former shows the highest retentivity and selectivity of the two, this in line with ^{1}NMR titration results and steric considerations. The strongest binding capability was seen for MIP28, grafted with the dicationic functional host monomer IMI5 by continuous radiation for 1 h, using the JD-230 Gel Curing Lamp as UV source. IMI5 has potential of presenting three positive charges by the *bis*-imidazolium and pyridine rings and showed the second-highest retention factor (31.7) of the set, together with the highest imprinting, selectivity, and relative imprinting factors of 3.71, 0.93 and 0.96, respectively. This high specificity made us choose the IMI5 grafted MIP28 for further investigations in the following practical chromatographic separation step.

Chromatographic Evaluation of the Optimal Monolithic Capillary Columns. We first consider the retention patterns under an isocratic elution for the relatively uncomplicated *N*-Fmoc protected amino acids, Fmoc-S-OH, Fmoc-Y-OH, Fmoc-**pS**-OH, and Fmoc-**pY**-OH on the TRIM24 capillary monolith substrate and the NIP and MIP prepared according to the MIP28 recipe. Their elution profiles using high organic (90 % ACN) and mainly aqueous (10 % ACN) mobile phases are shown in Figure 2.

It is obvious that the ungrafted TRIM monolith lacked recognition capability and exhibited minimal non-specific interactions, since all the amino acids eluted close to the void volume as sharp peaks in both these mobile phases of widely different polarity. By comparison, the NIP showed relatively longer analyte retention time and a slight discrimination between the non-phosphorylated and phosphorylated Fmoc amino acids, especially when eluted by 10 % ACN in HEPES buffer, pH 7.4. This verifies that the grafting step had changed the surface properties of the TRIM substrate monoliths. Moreover, neither of these elution conditions yielded recognition capability for the Fmoc protected phosphorylated serine. This suggests the existence of a certain level of non-specific interactions due to the potential electrostatic, hydrogen bonding, and π–π stacking multiple interactions between the phosphorylated Fmoc amino acids and monomers. On the MIP monolith, all the Fmoc-protected amino acid probes, unphosphorylated as well as phosphorylated, showed significant retention with both mobile phases, although the retention of the phosphorylated counterparts was substantially higher. It is thereby evident that the capillary monolith targeting **pS** by photoinitiated oriented surface cryoimprinting displayed a strong and specific retention for the corresponding phosphorylated amino acid under these radically different solvent conditions.

It is important to recall that this **pS** recognition capability was specific for the imprinted epitope, *i.e.*, Fmoc-**pS**-OH had higher retention than Fmoc-**pY**-OH on the MIP monolith in both the organic and aqueous rich mobile phases. This is especially encouraging, since the use of aromatic monomers did not create a non-specific selectivity for aromatic groups; neither for the aryl group of the tyrosine, nor for the Fmoc protective group as we saw in our previous work based on direct imprinting by polymerization of melamine-formaldehyde.[32]

Turning to the intended use of the imprinted monolith in phosphopeptides trapping, we thereafter challenged the MIP and NIP with a suite of more complex sample represented by human Angiotensin II

with (DRV**pY**IHPF) and without (DRVYIHPF) phosphorylation on tyrosine, and its homologs (DRV**pS**IHPF and DRVSIHPF) with **pS**/S substituted for **pY**/Y. When a mixture of these peptides was injected, the phosphorylated octapeptides, especially DRV**pS**IHPF, showed a retention pattern on the MIP monolith with peaks featuring a weak albeit characteristic "MIP tailing"; *cf.* Figure 3.

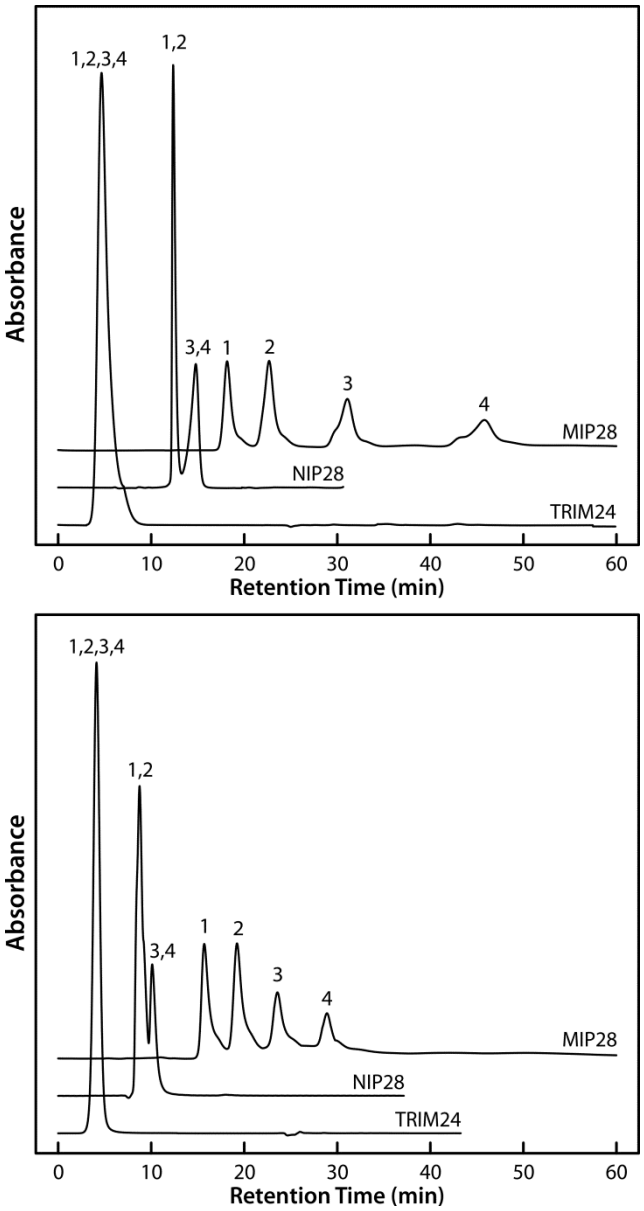

Figure 2. μ-LC chromatograms of Fmoc protected amino acids on the capillary monoliths. Peaks: Fmoc-S-OH (1); Fmoc-Y-OH (2); Fmoc-**pY**-OH (3); Fmoc-**pS**-OH (4). Mobile phases: Top, ACN/H_2O (0.1% TFA) (90:10, v/v); bottom, ACN/100 mM aqueous HEPES buffer, pH 7.4 (10:90, v/v); flow rate, 4 μL/min; UV detection at 254 nm; injection volume, 35 nL.

Again we see characteristic imprinting effects and similarly strong selectivites in both the mainly organic and aqueous mobile phases. In other words, distinct high affinities were observed for the peptide phosphorylated on serine (DRV**pS**IHPF) on the imprinted capillary monoliths compared to its NIP counterpart, let alone the TRIM monolith substrate which showed no specific affinity. These results prove that photo-initiated oriented surface cryoimprinting using a single amino acid as a template can be used to create a site-specific **pS** capture phase capable of trapping octapeptides, even when the phosphorylation site is located well away from the terminals. It is particularly noteworthy that the DRV**pS**IHPF, phosphorylated on serine, had a higher retention than the DRV**pY**IHPF phosphotyrosine analogue also in this set of probes, showing that the phosphoselectivity was specific to the **pS** motif. The a similar specificity for **pY** over **pS** was seen in our previous paper where *N*-Fmoc-*O*-ethyl protected phosphotyrosine was imprinted on monoliths prepared by step-growth polymerization of melamine and formaldehyde.[32]

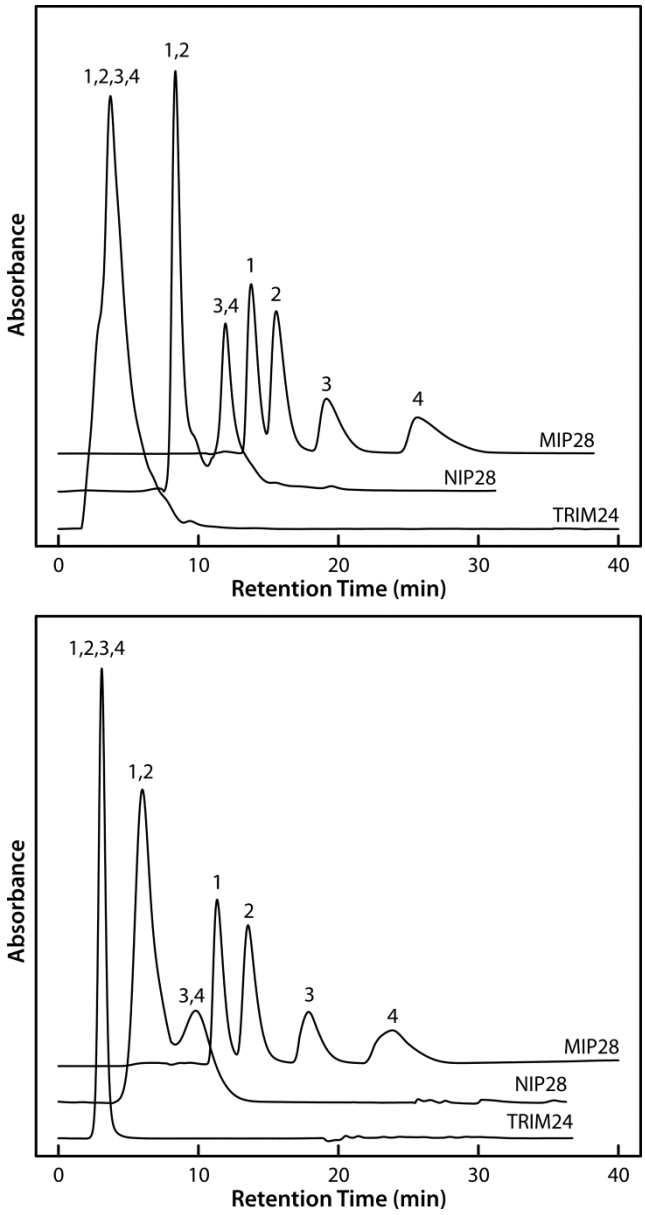

Figure 3. μ-LC chromatograms of a mixture of human Angiotensin II octapeptides on the capillary monoliths. Peptide peaks: DRVSIHPF (1); DRVYIHPF (2); DRV**pY**IHPF (3); DRV**pS**IHPF (4). μ-LC conditions as in Figure 2, except UV detection at 210 nm.

Verification of the pS Site-specific Peptide Recognition Specificity. In view of the promising results above, the trapping ability and selectivity of MIP28 for a sample of higher complexity was checked by a tryptic digest of α-casein, using an LTQ Orbitrap XL MS instrument which allowed us to identify a range of peptides of varying length, phosphorylated as well as non-phosphorylated due to its high accuracy and resolution. The results presented in Figure 4 show nine representative extracted ion chromatograms (EICs); the upper four from non-phosphorylated peptides of varying length, and the bottom five from peptides with varying level of phosphorylation, with the

programmed, steep gradient profile overlaid. Evident from these EICs is that all the non-phosphorylated peptides eluted around 10.5 minutes, independent of length. This must have been close to the start of the actual gradient considering the volume lag between the pump and the monolithic column, which was not known. The five phosphorylated peptides eluted at retention times which, as a general trend, became gradually longer with increasing number of phosphorylations. Multiphosphorylation also caused the peaks to become wider, indicating that peptides with more than one phospho group were forced to utilize more than one binding site, where the non-predetermined spatial distribution caused a greater variability in binding strength.

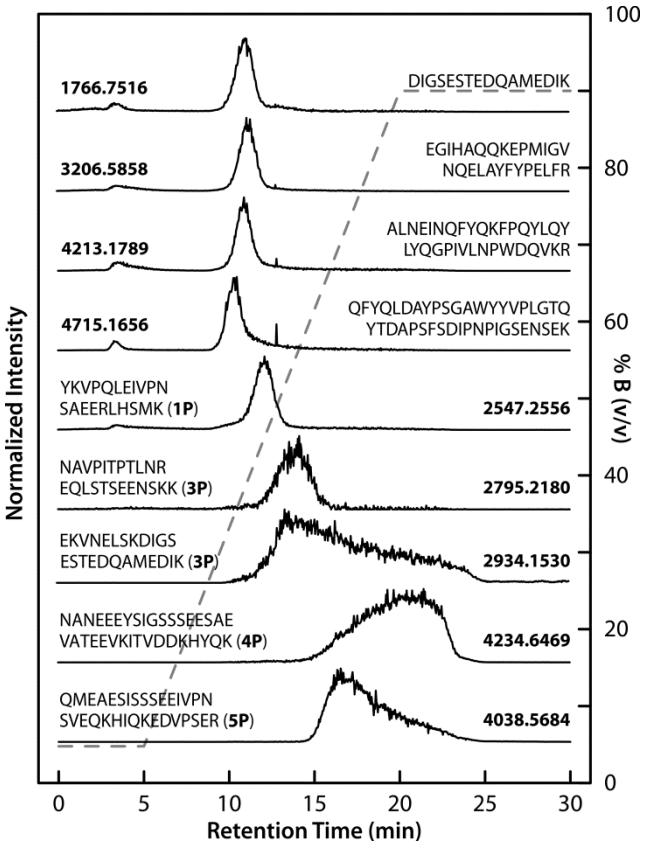

Figure 4. Extracted ion chromatograms of four representative non-phosphorylated peptides of varying length (upper traces with annotated masses to the left and amino acid sequence to the right) and five peptides of varying phosphorylation levels (lower traces with annotated masses to the right and amino acid sequence to the left) from a tryptic digest of α-casein, separated on the optimized MIP monolithic capillary column. The dashed line shows the programmed binary gradient from 95 % mobile phase A (pure acetonitrile), to 90 % mobile phase B (20 mM formic acid in water).

Modeling of the retention of the α-casein tryptic digest peptides against parameters which, at least in some sense describe their properties, was finally carried out by projection against latent structures (PLS) in SIMCA 15.0 (Umetrics, Umeå, Sweden). The explanatory variables were aliphatic index, GRAVY, the calculated pI, and the molecular weights (MW) for the non-phosphorylated peptides, the number of phosphorylations, and the count of each of the twenty common amino acids as scaled numerical variables. This led to an overfitted model which failed to show any relationships. A reduced PLS model was therefore established with all amino acids except those with charged side chains (Arg, Asp, Glu, and Lys) removed. Aliphatic index and GRAVY were both allowed to remain in the modified model, since the correlation between these two hydrophobicity indices was surprisingly low (Pearson $r^2 = 0.29$).

They also seemed to explain different aspects of the peptides, since they appeared well separated in the biplot. A PLS model with the two first components forced is shown in Figure 5 as a "biplot" of loadings and scores, in order to visualize the connections between the fundamental properties of the peptides and their parameters derived from ExPaSy ProtParam, and the observed retentions of the identified peptides in a single plot.

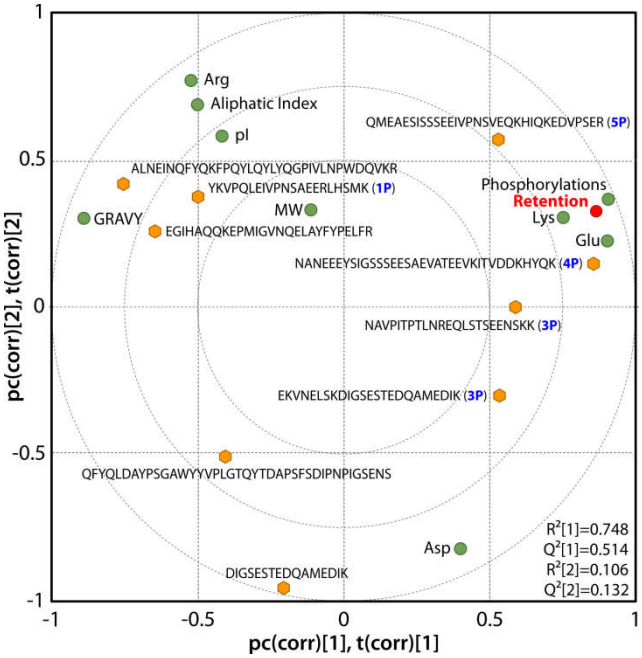

Figure 5. Biplot of the scores and loadings of a projection against latent structures (PLS) model of the retention of unphosphorylated and phosphorylated peptides found in an α-casein tryptic digest (yellow hexagons), using as explaining variables computed values of pI, aliphatic index, and grand average of hydropathicity (GRAVY) of the identified peptides in their non-phosphorylated state obtained from ExPaSy ProtParam, along with the number of charged amino acids in the peptide sequence (Arg, Lys, Glu, and Asp), all plotted as green circles. The number of phosphorylations is shown in parentheses after the peptide sequences. A color graphic is found in the PDF version.

This PLS model explained some 85 % of the variation contained in the data. Clear from this plot, where most of the variation ($R^2 = 0.748$) is explained in the horizontal dimension, is that the observed retentions are strongly correlated with the number of phosphorylated residuals. The retention interestingly also show equally strong positive correlations with the number of the amino acids glutamic acid and lysine. The retention is moreover inversely correlated with GRAVY and Aliphatic Index, which means that the peptides are better retained, the less hydrophobic they are. The retention also appears to be unrelated to the size of the peptide, since MW is located close to the center of the plot.

A hierarchical cluster model classifies all phosphopeptides except YKVPQLEIVPNSAEERLHSMK (1P) in one cluster, and this monophopsphorylated peptide and all the unphosphorylated peptides in another cluster. On a lower hierarchical level, the longest and shortest of the non-phosphorylated peptides comprised a single cluster, well separated from the other, further verifying that the observed retention was not due to peptide size.

■ CONCLUSIONS

Surface imprinted capillary monoliths targeting phosphorylated serine have been prepared by grafting custom imidazolium monomers onto monolithic substrates. Both the preparation of the TRIM-based grafting substrates and the oriented surface imprinting was carried out

by photo-initiated cryopolymerization. The molecularly imprinted capillary monoliths synthesized under optimized conditions exhibited highly selective affinity for phosphorylation of serine. The efficient and timesaving synthesis method opens a new avenue for preparation of synthetic affinity materials of high selectivity. The successful specific separation applications suggest that the synthesized monolithic plastic antibodies can be developed into a promising tool in the context of complex phosphoproteomic analysis and extended clinical screening diagnosis.

■ ASSOCIATED CONTENT

Additional reagents; experimental details, background information, and results for the characterization experiments in Figures S-1 to S-8 and Tables S-1 to S-3. This material is available free of charge via the Internet at http://pubs.acs.org.

■ AUTHOR INFORMATION

Corresponding Author

* Phone: +46 90 7865997; e-mail: knut.irgum@chem.umu.se

Present Addresses

¶ Department of Neurology, Akershus University Hospital, Sykehusveien 25, N-1478 Lørenskog, Norway.

Author Contributions

The manuscript was written with contributions of all authors, who have all given their approval to the final version of the manuscript.

Funding Sources

Marie Curie ITN project *"Robust affinity materials for applications in proteomics and diagnostics"* project PEPMIP, supported by European Commission grant PITN-GA-2010-569 264699.

Conflict of Interest Statement

The authors declare no competing financial interest.

■ ACKNOWLEDGMENT

The authors are indebted to Ignacio Arribas Díez, Julien Courtois, Wen Jiang, Michał Szumski, Shaochun Zhu, Jing Chen, Thomas Kieselbach, and Sudhirkumar Shinde for discussions throughout this work. The authors also acknowledge the valuable technical assistance of Cheng Choo Lee, Tobias Sparrman, Andras Gorzsas, Andrey Shchukarev, Robin Sandström, and Thomas Wågberg.

■ REFERENCES

(1) Johnson, S. A.; Hunter, T. *Nat. Methods* **2005**, 2, 17-24.
(2) Macek, B.; Gnad, F.; Soufi, B.; Kumar, C.; Olsen, J. V.; Mijakovic, I.; Mann, M. *Mol. Cell. Proteomics* **2008**, 7, 299-307.
(3) Mazanetz, M. P.; Fischer, P. M. *Nat. Rev. Drug Discovery* **2007**, 6, 464-479.
(4) Ruprecht, B.; Lemeer, S. *Expert Rev. Proteomics* **2014**, 11, 259-267.
(5) Rush, J.; Moritz, A.; Lee, K. A. Guo, A.; Goss, V. L.; Spek, E. J.; Zhang, H. X.; Zha, X.-M.; Polakiewicz, R. D.; Comb, M. J. *Nat. Biotechnol.* **2005**, 23, 94-101.
(6) Larsen, M. R.; Thingholm, T. E.; Jensen, O. N.; Roepsdorff, P.; Jørgensen, T. J. D. *Mol. Cell. Proteomics* **2005**, 4, 873-886.
(7) Li, X.-S.; Yuan, B.-F.; Feng, Y.-Q. *Trac-Trends Anal. Chem.* **2016**, 78, 70-83.
(8) Zhang, X.; Ye, J. Y.; Jensen, O. N.; Roepstorff, P. *Mol. Cell. Proteomics* **2007**, 6, 2032-2042.
(9) Zhou, H. L.; Watts, J. D.; Aebersold, R. *Nat. Biotechnol.* **2001**, 19, 375-378.
(10) Dong, M. M.; Wu, M. H.; Wang, F. J.; Qin, H. Q.; Han, G. H.; Dong, J.; Wu, R. A.; Ye, M. L.; Liu, Z.; Zou, H. F. *Anal. Chem.* **2010**, 82, 2907-2915.
(11) Pinto, G.; Caira, S.; Cuollo, M.; Lilla, S.; Fierro, O.; Addeo, F. *J. Chromatogr. B* **2010**, 878, 2669-2678.
(12) Leitner, A. *Trac-Trends Anal. Chem.* **2010**, 29, 177-185.
(13) Bodenmiller, B.; Mueller, L. N.; Mueller, M.; Domon, B.; Aebersold, R. *Nat. Methods* **2006**, 4, 231-237.
(14) Ballif, B. A.; Carey, G. R.; Sunyaev, S. R.; Gygi, S. P. *J. Proteome Res.* **2008**, 7, 311-318.
(15) Thingholm, T.; Jensen, O. N.; Larsen, M. *Proteomics* **2009**, 9, 1451-1468.
(16) Thingholm, T.; Jorgensen, T.; Jensen, O. N.; Larsen, M. *Nat. Protoc.* **2006**, 1, 1929-1935.
(17) Villen, J.; Steven, P. G. *Nat. Protoc.* **2008**, 3, 1630-1638.
(18) Zarei, M.; Sprenger, A.; Metzger, F.; Gretzmeier, C.; Dengjel, J. *J. Proteome Res.* **2011**, 10, 3474-3483.
(19) Oda, Y.; Nagasu, T.; Chait, B. T. *Nat. Biotechnol.* **2001**, 19, 379-382.
(20) Grønborg, M.; Kristiansen, T. Z.; Stensballe, A.; Andersen, J. S.; Ohara, O; Mann, M.; Jensen, O. N.; Pandey, A. A *Mol. Cell Proteomics* **2002**, 1, 517-527.
(21) Bie, Z. J.; Chen, Y.; Ye, J.; Wang, S. S.; Liu, Z. *Angew. Chem. Int. Ed.* **2015**, 54, 10211-10215.
(22) Muhammad, P.; Tu, X. Y.; Liu, J.; Wang, Y. J.; Liu, Z. *ACS Appl. Mater. Interfaces* **2017**, 9, 12082-12091.
(23) Xing, R. R.; Wang, S. S.; Bie, Z. J.; He, H.; Liu, Z. *Nat. Protoc.* **2017**, 12, 964-987.
(24) Adali-Kaya, Z.; Bui, B. T. S.; Falcimaigne-Cordin, A.; Haupt. K. *Angew. Chem. Int. Ed.* **2015**, 54, 5192-5195.
(25) Shinde, S.; El-Schich, Z.; Malakpour, A.; Wan, W.; Dizeyi, N.; Mohammadi, R.; Rurack, K.; Wingren, A. G.; Sellergren, B. *J. Am. Chem. Soc.* **2015**, 137, 13908-13912.
(26) Liu, Z.; He, H. *Acc. Chem. Res.* **2017**, 50, 2185-2193.
(27) Chen, L. X.; Wang, X. Y.; Lu, W. H.; Wu, X. Q.; Li, J. H. *Chem. Soc. Rev.* **2016**, 45, 2137-2211.
(28) Pan, X. H.; He, X. P.; Liu, Z. *Anal. Chim. Acta* **2018**, 1019, 65-73.
(29) Chen, J.; Shinde, S.; Koch, M.-H.; Eisenacher, M.; Galozzi, S.; Lerari, T.; Barkovits, K.; Subedi, P.; Krüger, R.; Kuhlmann, K.; Sellergren, B.; Helling, S.; Marcus, K. *Sci. Rep.* **2015**, 5, 11438, 12 pp.
(30) Svec, F.; Lv, Y. Q. *Anal. Chem.* **2015**, 87, 250-273.
(31) Masini, J. C.; Svec, F. *Anal. Chim. Acta* **2017**, 964, 24-44.
(32) Liu, M. Q.; Tran, T. M.; Elhaj, A. A. A.; Torsetnes, S. B.; Jensen, O. N.; Sellergren, B.; Irgum, K. *Anal. Chem.* **2017**, 89, 9491-9501.
(33) Courtois, J.; Fischer, G.; Sellergren, B.; Irgum, K. *J. Chromatogr. A* **2006**, 1109, 92-99.
(34) Emgenbroich, M.; Borrelli, C.; Shinde, S.; Lazraq, I.; Vilela, F.; Hall, A. J.; Oxelbark, J.; De Lorenzi, E.; Courtois, J.; Simanova, A.; Verhage, J.; Irgum, K.; Karim, K.; Sellergren, B. *Chem. Eur. J.* **2008**, 14, 9516-9529.
(35) Wierzbicka, C.; Liu, M.; Bauer, D.; Irgum, K.; Sellergren, B. *J. Mater. Chem. B* **2017**, 5, 953-960.
(36) Sulc, R.; Szekely, G.; Shinde, S.; Wierzbicka, C.; Vilela, F.; Bauer, D.; Sellergren, B. *Sci. Rep.* **2017**, 7, 44299, 10 pp.
(37) Narayanaswamy, P.; Shinde, S.; Sulc, R.; Kraut, R.; Staples, G.; Thiam, C. H.; Grimm, R.; Sellergren, B.; Torta, F.; Wenk, M. R. *Anal. Chem.* **2014**, 86, 3043-3047.
(38) Shinde, S.; Bunschoten, A.; Kruijtzer, J. A. W.; Liskamp, R. M. J.; Sellergren, B. *Angew. Chem., Int. Ed.* **2012**, 51, 8326-8329.
(39) Wouters. S.; Hauffman, T.; Hazeleger, M. C. M.; Rothenberg, G.; Desmet, G.; Baron, G. V.; Eeltink, S. *J. Sep. Sci.* **2016**, 39, 4492-4501.

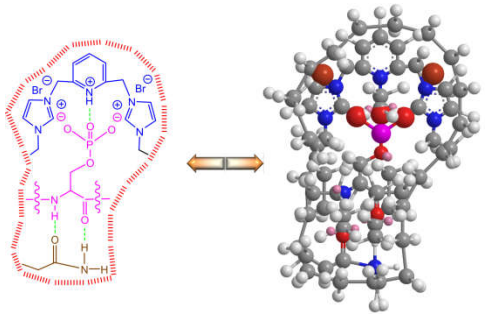

Table of Contents Artwork